Computing Systems in Engineering Vol. 3, Nos 1–4, pp. 153–168, 1992
Printed in Great Britain.

0956-0521/92 $5.00 + 0.00
© 1992 Pergamon Press Ltd

RE-INVENTING ELECTROMAGNETICS: SUPERCOMPUTING SOLUTION OF MAXWELL'S EQUATIONS VIA DIRECT TIME INTEGRATION ON SPACE GRIDS

A. TAFLOVE
Department of Electrical Engineering and Computer Science, McCormick School of Engineering, Northwestern University, Evanston, IL 60208-3118, U.S.A.

Abstract—This paper summarizes the present state and future directions of applying finite-difference and finite-volume time-domain techniques for Maxwell's equations on supercomputers to model complex electromagnetic wave interactions with structures. Applications so far have been dominated by radar cross-section technology, but by no means are limited to this area. In fact, the gains we have made place us on the threshold of being able to make tremendous contributions to non-defense electronics and optical technology. Some of the most interesting research in these commercial areas is summarized.

1. INTRODUCTION

Defense requirements for aerospace vehicles having low radar cross-section (RCS) have driven the development of large-scale methods in computational electromagnetics. We have an anomaly that the effectiveness and cost of such state-of-the-art systems depends upon our ability to develop engineering understanding of century-old basic science, Maxwell's equations (*ca* 1870). Recently, direct space-grid time-domain Maxwell's solvers have been the subject of intense interest for this application, challenging previously dominant frequency-domain integral equation approaches.

This paper summarizes the history, present state, and possible future of applying space-grid time-domain techniques for Maxwell's equations to model complex electromagnetic wave interactions. As teraflop-class supercomputers permit structures of amazing complexity and size to be modeled, the old/new theme of Maxwell's equations/RCS design will be seen to recur in areas that cut a wide swath through the core of electrical engineering. We will consider:

- The state of the full-matrix method of moments.
- The history of space-grid time-domain techniques for Maxwell's equations.
- The state of existing algorithms and meshes: basis, primary types, predictive dynamic range.
- Scaling to problems of $>10^9$ field unknowns.
- Future defense electromagnetics needs: 70 dB dynamic range; modeling of complex and composite materials; optimization of materials and shapes for RCS; integrated RCS and aerodynamics design and optimization; target identification.
- Future dual-use electromagnetics needs: antenna design; microwave and millimeter wave integrated circuits; bio-electromagnetic systems; high-speed interconnects and packaging for electronic digital circuits; incorporation of models of active devices; all-optical devices, including femtosecond switches and logic gates.

Overall, advances in supercomputing solutions of Maxwell's equations based on their direct time integration on space grids place us on the threshold of being able to make large contributions to dual-use electronics and optical technology as well as RCS technology. In fact, I claim that solving Maxwell's equations at ultra-large scales will permit us to design devices having working bandwidths literally from d.c. to light.

2. THE STATE OF THE FULL-MATRIX METHOD OF MOMENTS

The modeling of engineering systems involving EM wave interactions has been dominated by frequency-domain integral equation techniques and high-frequency asymptotics. This is evidenced by the almost universal use of the method of moments (MoM)[1,2] to provide a rigorous boundary value analysis of structures and the geometrical theory of diffraction (GTD)[3,4] to provide an approximate analysis valid in the high-frequency limit. However, a number of important contemporary problems in EM wave engineering are not adequately treated by such models. Complexities of structure shape and material composition confound the GTD analysts; and structures of even moderate electrical size (spanning five or more wavelengths in three dimensions) present very difficult computer resource scaling problems for MoM.

The latter problem is particularly serious since MoM has provided virtually the only means of dealing with the non-metallic materials now

commonly used in aerospace design. Consider the following:

Define d_{span} as the characteristic span of a flat-configured target and λ_0 as the wavelength of the impinging radar beam such that the electrical surface area of the target (in square wavelengths) is $2(d_{span}/\lambda_0)^2$. Assume a standard triangular surface patching implementation of the electric field integral equation with the surface area of the target discretized at R divisions per λ_0. Then, the number of triangular surface patches is given by $4R^2(d_{span}/\lambda_0)^2$; and N, the number of field unknowns, is given by $6R^2(d_{span}/\lambda_0)^2$. In fact, N is the order of the MoM system matrix. With R usually taken as 10 or greater to properly sample the induced electric current distribution on the target surface, we see that N rises above 10,000 for d_{span} greater than $4\lambda_0$. Further, we see that N increases quadratically as λ_0 drops (radar frequency increases) and the computational burden for LU decomposition increases as the *sixth power* of frequency (order of N^3).

Let us see what this means in terms of program running time for the recently introduced CRAY C-90 supercomputer. First, assume that d_{span} is on the order of 10 m, perhaps typical of a jet fighter. N rises above 40,000 at a radar frequency of 240 MHz and the CRAY C-90 running time is projected to be less than 3 h, based upon much experience with the CRAY Y-MP/8 machine.[5] Up an octave to 480 MHz, N increases to 160,000 and the C-90 running time projects to be 8 days, a 64-fold (2^6) increase. Up still another octave to 960 MHz, N increases to 640,000 and the C-90 running time projects to be 1 year, 5 months. The latter assumes that: (a) we have enough disk drives to store the trillion-word MoM matrix; (b) we find acceptable the error accumulation resulting from the million-trillion floating-point operations on MoM matrix elements having precisions of only perhaps 1 part in 10,000; and (c) the computer system stays up continuously for over 1 year.

It is quite clear that the traditional, full-matrix MoM computational modeling of an entire aerospace structure such as a fighter plane is at present impractical at radar frequencies much above 500 MHz, despite advances in supercomputer hardware and software. However, radar frequencies of interest go much higher than 500 MHz, in fact up to 10 GHz or more. Much research effort has been expended in deriving alternative iterative frequency-domain approaches (conjugate gradient, spectral, etc.) that preserve the rigorous boundary-integral formulation of MoM while realizing dimensionally reduced computational burdens. These would permit, in principle, entire aircraft modeling at radar frequencies well above 500 MHz. However, these alternatives may not be as robust as the full-matrix MoM, that is, providing results of engineering value for a wide class of structures without the user wondering if the algorithm is converged.

3. HISTORY OF SPACE-GRID TIME-DOMAIN TECHNIQUES FOR MAXWELL'S EQUATIONS

The problems involved in applying frequency-domain, dense-matrix MoM technology to large-scale RCS modeling have prompted a rapid recent expansion of interest in an alternative class of non-matrix approaches: direct space-grid time-domain solvers for Maxwell's time-dependent curl equations. The new approaches appear to be as robust and accurate as MoM, but have dimensionally-reduced computational burdens to the point where whole-aircraft modeling for RCS is becoming possible at frequencies above 1 GHz. They are analogous to existing mesh-based solutions of fluid-flow problems in that the numerical model is based upon a direct, time-domain solution of the governing partial differential equation. Yet, they are very non-traditional approaches to CEM for engineering applications, where frequency-domain methods (primarily MoM) have dominated.

Table 1 summarizes key developments and publications in the history of direct space-grid time-domain solvers for Maxwell's time-dependent curl equations. As can be seen, both the pace and range of applications of FD-TD and other time-domain grid-based models of Maxwell's equations are expanding rapidly. These efficient volumetric solutions in the time domain are making possible applications in areas far beyond those of the method of moments. In this regard, this paper seeks to explore selected areas of high promise.

4. STATE OF EXISTING ALGORITHMS AND MESHES

4.1. *Basis*

FD-TD and FV-TD are direct solution methods for Maxwell's equations. They employ no potentials. Rather, they are based upon volumetric sampling of the unknown near-field distribution (E and H fields) within and surrounding the structure of interest, and over a period of time. The sampling in space is at a sub-wavelength (sub-λ_0) resolution set by the user to properly sample (in the Nyquist sense) the highest near-field spatial frequencies thought to be important in the physics of the problem. Typically, 10–20 samples per illumination wavelength are needed. The sampling in time is selected to insure numerical stability of the algorithm.

Overall, FD-TD and FV-TD are marching-in-time procedures which simulate the continuous actual EM waves by sampled-data numerical analogs propagating in a computer data space. Time-stepping continues as the numerical wave analogs propagate in the space grid to causally connect the physics of all regions of the target. All outgoing scattered wave analogs ideally propagate through the lattice truncation planes with negligible reflection to exit the region. Phenomena such as induction of surface currents, scattering and multiple scattering, aperture penetration and cavity excitation are modeled time

Table 1. Partial history of space-grid time-domain techniques for Maxwell's equations

1966	Yee[6] described the basis of the first space-grid time-domain technique, later called the finite-difference time-domain (FD-TD) method. FD-TD implements the spatial derivatives of the curl operators using finite differences in regular interleaved (dual) Cartesian space meshes for the electric and magnetic fields. Simple leapfrog time integration is employed
1975	Taflove and Brodwin published the correct numerical stability criterion for Yee's algorithm and the first grid-based time-integration of a two-dimensional EM scattering problem all the way to the sinusoidal steady state,[7] as well as the first three-dimensional grid-based computational model of EM wave absorption in complex, inhomogeneous biological tissues[8]
1977	Holland[9] and Kunz and Lee[10] applied the Yee algorithm to electromagnetic pulse (EMP) interaction problems
1980	Taflove coined the term "FD-TD" and published the first validated FD-TD models of EM wave penetration of a three-dimensional metal cavity[11]
1981	Mur published an accurate and numerically stable second-order radiation boundary condition for the Yee grid[12]
1982, 1983	Umashankar and Taflove published the first FD-TD EM wave scattering models computing near fields, far fields and RCS for two-dimensional structures[13] and three-dimensional structures[14]
1987, 1988	Kriegsmann and coworkers introduced modern radiation boundary condition theory to the engineering EM community[15,16]
1987–	Sullivan, Gandhi, Taflove and coworkers commenced publishing a series of articles applying FD-TD to model EM wave interactions, especially hyperthermia, with complex three-dimensional models of humans[17–20]
1987–	Taflove, Umashankar and coworkers introduced contour-path, subcell techniques to permit FD-TD modeling of EM wave coupling to thin wires and wire bundles,[21] EM wave penetration through cracks in conducting screens[22] and conformal surface treatments of curved structures[23]
1988–	Finite-element time-domain (FE-TD), body-fitted finite-volume time-domain (FV-TD) and unstructured or partially unstructured meshes for Maxwell's equations were introduced by Cangellaris *et al.*,[24] Shankar *et al.*,[25] McCartin *et al.*,[26] and Madsen and Ziolkowski[27]
1989–	FD-TD modeling of digital circuit interconnects and microstrips was introduced by Liang *et al.*,[28] Shibata and Sano,[29] Sheen *et al.*[30] and Ko and Mittra[31]
1990–	FD-TD modeling of frequency-dependent dielectric permittivity was introduced by Luebbers *et al.*,[32] and Joseph *et al.*[33]
1990–	FD-TD modeling of antennas was introduced by Maloney *et al.*,[34] Tirkas and Balanis[35] and Katz *et al.*[36]
1990–	FD-TD modeling of picosecond optoelectronic switches was introduced by Sano and Shibata[37] and El-Ghazaly *et al.*[38]
1991–	FD-TD modeling of the propagation of femtosecond optical pulses in non-linear dispersive media was introduced by Goorjian and Taflove[39] and Ziolkowski and Judkins[40]
1992–	FD-TD modeling of lumped-circuit elements (resistors, inductors, capacitors, diodes and transistors) in a two-dimensional EM wave code was introduced by Sui *et al.*[41]

step by time step by the action of the curl equations analog. Self-consistency of these modeled phenomena is generally assured if their spatial and temporal variations are well resolved by the space and time sampling process. In fact, the goal is to provide a self-consistent model of the mutual coupling of all of the electrically-small volume cells comprising the structure and its near field, even if the structure spans tens of λ_0 in three dimensions and there are tens of millions of space cells.

Time-stepping is continued until the desired late-time pulse response or steady-state behavior is observed. An important example of the latter is the sinusoidal steady state, wherein the incident wave is assumed to have a sinusoidal dependence and time-stepping is continued until all fields in the sampling region exhibit sinusoidal repetition. This is a consequence of the limiting amplitude principle. Extensive numerical experimentation has shown that the number of complete cycles of the incident wave required to be time-stepped to achieve the sinusoidal steady state is a function of:

(1) *Target electrical size*. For many targets, this requires a number of time steps sufficient to permit at least two front-to-back-to-front traverses of the target by a wave analog. For example, assuming a target spanning $10\lambda_0$, at least 40 cycles of the incident wave should be time-stepped to approach the sinusoidal steady state. For a grid resolution of $\lambda_0/10$, this corresponds to 800 time steps for FD-TD.

(2) *Target* Q *factor*. Targets having well-defined low-loss cavities or low-loss dielectric compositions may require the number of complete cycles of the incident wave to be time-stepped to approach the Q factor of the resonance; because Q can be large even for electrically moderate size cavities, this can dictate how many time steps the FD-TD or FV-TD code must be run.

In the RCS area, target electrical size may often be the dominant factor. Cavities for RCS problems (such as engine inlets) tend to be open and therefore moderate Q; and the use of radar-absorbing material (RAM) serves further to reduce the Q factors of structures.

4.2. *Primary types*

The primary FD-TD and FV-TD algorithms used today are fully explicit second-order accurate grid-based solvers employing highly vectorizable and concurrent schemes for time-marching the six vector components of the EM near field at each of the

volume cells. The explicit nature of the solvers is maintained by either leapfrog or predictor–corrector time integration schemes. Second-order accurate radiation boundary conditions are used to simulate the extension of the problem space to infinity, thereby minimizing error due to the artifactual reflection of outgoing numerical wave modes at the mesh outer boundary.

Present methods differ primarily in how the space grid is set up. In fact, gridding methods can be categorized according to the degree of structure or regularity in the mesh:

(1) *Almost completely structured.* Space cells more than one or two cells from the structure of interest are organized in a completely regular manner, for example, using a uniform Yee Cartesian mesh. Only the cells adjacent to the structure are modified in size and shape to conformally fit the structure surface.[23,27]

—Advantage: computationally efficient, because there are relatively few modified cells requiring special storage to locate the cells in the mesh and special computations to perform the field updates. In fact, the number of modified cells (proportional to the surface area of the structure) becomes arbitrarily small compared with the number of regular mesh cells as structure size increases. As a result, the computer memory and running time needed to implement a fully conformal model can be indistinguishable from that required for a stepped-surface model. Further, an ultra-fast, minimal memory, Yee-like algorithm can be used for the regular space cells.

—Advantage: mapping of the mesh onto a parallel–vector computer or massively parallel computer is straightforward.

—Advantage: artifacts due to refraction and reflection of numerical wave modes propagating across global mesh distortions are not present. This is especially important for three-dimensional structures having substantial EM coupling between electrically disjoint sections, or reentrant regions.

—Disadvantage: geometry generation software for this type of meshing has not reached the mature state achieved for other types. Considerable work remains.

—Disadvantage: thin target surface coatings do not conform to mesh boundaries. These are best modeled here using surface impedances.

(2) *Body-fitted.* The space grid is globally distorted to fit the shape of the structure of interest.[25] Effectively, a coordinate transformation between a non-Cartesian physical mesh and a Cartesian logical mesh is implemented.

—Advantage: well-developed geometry generation software is available from the CFD community. Aerodynamic shapes appropriate for the RCS problem are nicely handled.

—Advantage: thin target surface coatings naturally conform to mesh boundaries.

—Advantage: mapping of the logical mesh onto a parallel–vector computer or massively parallel computer is straightforward.

—Disadvantage: relative to the baseline Yee algorithm, extra computer storage must be allocated to account for the three-dimensional position and stretching factors of each space cell. Further, extra computer arithmetic operations must be performed to implement Maxwell's equations at each cell and/or to enforce EM field continuity at the interfaces of adjacent cells. As a result, the number of floating point operations needed to update the six field components at a space cell over one time step can exceed that of the Yee algorithm by as much as 20:1, thereby increasing running times by the same amount with respect to FD-TD.

—Disadvantage: artifacts due to refraction and reflection of numerical wave modes propagating across global mesh distortions will be present. These errors arise because the phase velocity of numerical wave modes propagating in the mesh is a function of position in the mesh, as well as angle of propagation. These artifacts are important for three-dimensional structures having substantial EM coupling between electrically disjoint sections, or reentrant regions, and may limit the predictive dynamic range (thereby limiting the ability to model low-observable structures).

(3) *Completely unstructured.* The space containing the structure of interest is completely filled with a collection of solid cells of varying sizes and shapes, but conforming to the structure surface.[26]

—Advantage: geometry generation software is available. This software is appropriate for modeling extremely complicated three-dimensional shapes possibly having volumetric inhomogeneities, for example inhomogeneous radar absorbing material.

—Disadvantages: the same as for the body-fitted meshes.

—Another disadvantage: mapping of the logical mesh onto a parallel–vector computer or massively parallel computer is not straightforward.

At present, the optimal choice of computational algorithm and mesh is not obvious. Clearly, there are important tradeoff decisions to be made. For the next several years, we can expect considerable progress in this area as various groups develop their favored approaches and perform validations.

4.3. *Predictive dynamic range*

For computational modeling of the RCS of aerospace vehicles (especially low-observable vehicles) using space-grid time-domain codes, it is useful to define a predictive dynamic range, D, analogous to the "quiet zone" figure of merit for an experimental anechoic chamber:

$$D = 10 \log(P^{\text{inc}}/P^{\text{scat,min}}) \text{ decibels,}$$

where P^{inc} is the power density of a modeled incident plane wave in the space grid, and $P^{scat,min}$ is the minimum observable local power density of a modeled scattered wave at any bistatic angle. At levels lower than this the accuracy of the computed scattered field degrades to poorer than 1 dB (or some other criterion).

This definition succinctly quantifies the reality that weak, physical numerical wave analogs propagating in the space grid exist in an additive noise environment due to the non-physical propagating wave analogs caused by the imperfect radiation boundary conditions. In addition to additive noise, the desired physical wave analogs undergo gradual progressive deterioration while propagating due to accumulating numerical dispersion artifacts, including phase velocity anisotropies and inhomogeneities within the mesh.

Since 1982, researchers have accumulated solid evidence for a predictive dynamic range of the order of 40 dB for the present class of second-order accurate space-grid time-domain codes when used to calculate monostatic and bistatic RCS. This value is reasonable if one considers the additive noise due to imperfect radiation boundaries to be the primary limiting factor, since existing second-order radiation boundary conditions yield effective reflection coefficients of about 1% (−40 dB), with an additional factor of perhaps −10 dB provided by the normal $r^{-1/2}$ rolloff (in two dimensions) or r^{-1} rolloff (in three dimensions) experienced by the outgoing scattered waves before reaching the radiation boundaries. Figure 1 illustrates a typical result for bistatic RCS dynamic range when using Cartesian-grid FD-TD with automated local mesh contouring to conform to curved target surfaces. Here, the scattering geometry consists of two 1 λ_0-diameter metal spheres separated by 1 λ_0 air gap, and the FD-TD grid has a uniform space resolution of 0.05 λ_0. The benchmark data are provided by a quasi-analytic frequency-domain approach, the generalized multipole technique (GMT).[42]

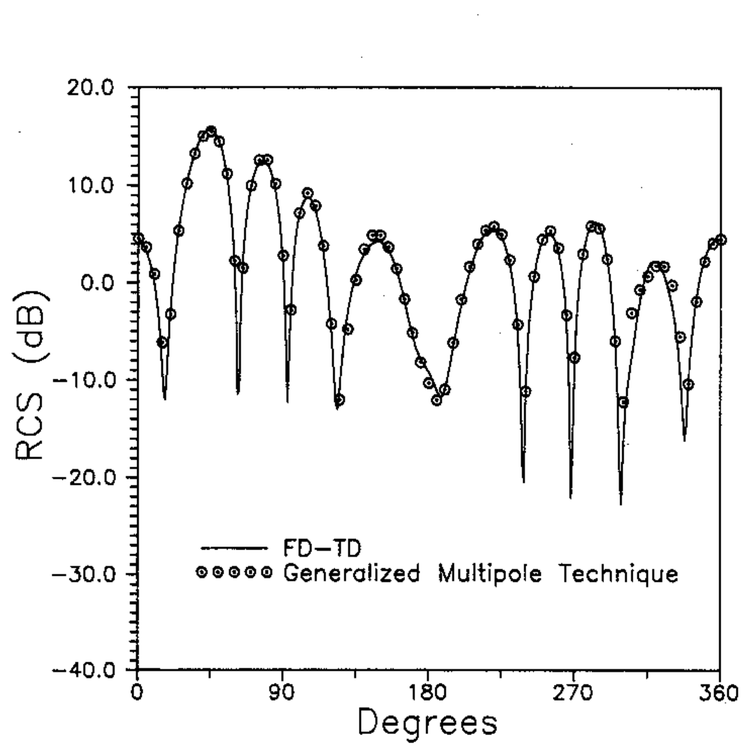

Fig. 1. Comparison of FD-TD and generalized multipole technique data for the bistatic RCS of two 1-λ diameter spheres separated by a 1-λ air gap, illuminated at oblique incidence.

Is more dynamic range needed? Certainly yes, if a better job is to be done in modeling specially shaped targets having low observability features. A good example of such a shape is the NASA almond,[43] which has been demonstrated to have monostatic RCS variations of 60 dB or more occurring over broad angular ranges. However, going from 40 to 60 or 70 dB will not be simple: We will require the development of advanced radiation boundary conditions having effective reflection coefficients of 0.1% or better, thereby reducing this contribution to the grid noise by 20 dB or more; and we will have to shift to space-sampling, time-integration algorithms having dimensionally better accuracy than the second-order procedures common today. A 20 dB reduction in the grid noise contribution due to dispersive effects accumulating on propagating numerical waves is needed to permit the use of grid resolutions no finer than those of today's algorithms.

5. SCALING TO PROBLEMS OF GREATER THAN 10^9 FIELD UNKNOWNS

5.1. *Why this problem size is needed*

Three-dimensional electromagnetic wave interaction problems modeled on volumetric space grids at the size level of 10^9 unknowns begin to have major engineering applications. For example, these might include: entire fighter planes illuminated by radar at 1 GHz and above; entire personal-computer-size multi-layer circuit boards modeled layer by layer for digital signal propagation, crosstalk and radiation; and entire microstrip circuits and antennas.

At this level, the goals are to achieve algorithm/computer architecture scaling such that for N field unknowns to be solved on M processors, we wish to approach an order (N/M) scaling of the computational modeling time.

5.2. *Algorithm scaling factors*

Is there a "best" EM computational algorithm to approach the ideal order (N) scaling of the computational modeling time? A consensus appears to be emerging that the class of non-matrix, space-grid time-domain solvers has the most promise. If robust algorithms for spatial or domain decomposition[44] cannot be achieved, the class of matrix-based frequency-domain methods may fade as a viable alternative because of difficult computational and error propagation problems associated with any large matrix, whether dense or sparse.

Let us now consider the factors involved in determining the computational burden for the class of non-matrix, space-grid time-domain solvers.

(1) *Number of grid cells*, N. The six vector electromagnetic field components located at each grid cell must be updated at every time step. This yields by itself an order (N) scaling.

(2) *Number of time steps*. A completely self-consistent solution in the time domain mandates that

numerical wave analogs propagate over time scales sufficient to causally connect each portion of the structure of interest. Therefore, in three dimensions, it can be argued that the number of time steps increases as a characteristic electrical length of the structure and thus a fractional power function of N such as $N^{1/3}$. The number of time steps must also be adequate to march through "ring-up" and "ring-down" times of energy storage features such as cavities and cavity-backed apertures.

(3) *Cumulative propagation errors.* Additional computational burdens may arise due to the need for either progressive mesh refinement or progressively higher-accuracy algorithms to bound cumulative positional/phase errors for propagating numerical modes in progressively enlarged meshes. Any need for progressive mesh refinement would feed back to Factor 1.

It appears likely that for most RCS problems, Factors 2 and 3 will be weaker functions of the size of the modeled structure than Factor 1. This is because geometrical scattering features at increasing electrical distances from each other become more and more weakly coupled due to radiative and other losses acting on electromagnetic wave energy propagating between these features. However, at this time there is insufficient experience in the grid-based modeling community with three-dimensional structures in this electrically-large size regime to provide meaningful comment.

5.3. *Computer architecture scaling factors*

Is there a "best" computer architecture to approach the ideal 1/order(M) scaling of the computational modeling time as the number of processors, M, increases? At present, the optimum connectivity of multi-processors is not clear. In 1993, the following manufacturers will offer massively parallel machines of varying architectures having claimed peak performances exceeding 100 Gflops (0.1 Tflop):

Intel:	Paragon
Cray Research:	MPP0
Thinking Machines:	CM-5.

In addition, Cray Research continues to develop its line of conventional general purpose vector-processing supercomputers descending from the CRAY Y-MP and C-90 machines. This will lead to a 100 + Gflop general purpose machine, the CRAY C-95, in 1994–1995.

5.4. *Results to date*

A number of groups have implemented large-scale grid-based Maxwell's equation solvers on vector-processing and massively parallel supercomputers.[5,25,45–47] Sufficient experience has been accumulated to justify the following statements:

(1) Concurrencies very close to 100% (i.e. an algorithm speedup factor equal to eight if the number of available processors equals eight) have been achieved with the CRAY Y-MP/8 under the CRAY autotasking (automatic multitasking) compiler for FD-TD and FV-TD. Average processing rates exceeding 1.6 Gflops were achieved for full FORTRAN programs. Performance scaling looks excellent at least through 16 high-performance (CRAY C-90 class) processors.

(2) Good to very good concurrencies for FD-TD can also be achieved using the JPL/Intel Hypercube. Performance scaling looks good into the hundreds of moderate-performance (Intel I-860 class) processors.

(3) For grid-based Maxwell's solvers, the CRAY Y-MP and JPL/Intel Hypercube machines were much easier to program and achieved substantially better fractions of their peak speeds than the CM-2 Connection Machine, when the CM-2 was programmed using the PARIS assembler.

(4) The volumetric space-grid time-domain solvers are already more efficient than surface-patching MoM. In one example,[5,47] FD-TD was used to conformally model an electrically large ($25\,\lambda_0 \times 10\,\lambda_0 \times 10\,\lambda_0$) three-dimensional serpentine jet engine inlet. Here, the projected CRAY C-90 time is only 30 s per illumination angle (involving time-marching 23,000,000 vector field components over 1800 time steps), or 1.6 days for 5000 angles. In comparison, the standard full-matrix MoM set up a dense matrix of approximately 450,000 equations, assuming that the 1500 λ_0^2 area of the engine inlet is discretized at 10 divisions per λ_0. The projected CRAY C-90 running time for LU decomposition and backsolve of this matrix is about 4 months for 5000 angles. Overall, the speedup when using FD-TD would be at least 75:1, with speedup factors much larger than this if we account for the likelihood of using FD-TD to evaluate the inlet RCS simultaneously for many frequencies by using an impulsive excitation and discrete Fourier transformation of the scattered field.

5.5. *The jet fighter model*

Consider again modeling a jet fighter, but now in the context of FD-TD. Assuming dimensions of $20 \times 20 \times 5$ m for the space grid and assuming a radar frequency of 1 GHz ($\lambda_0 = 0.3$ m; resolution = 3 cm), the space grid would be of the order of 75,000 λ_0^3 (450,000,000 vector field components) and the FD-TD central memory requirement would be about 1.3 Gword. This central memory size is currently feasible with 1–4 billion-word memory options of the CRAY Y-MP series. Running time on the C-90 is projected to be in the range 20–25 min per illumination angle. Modeling of the fighter at radar frequencies of 2 GHz and higher would be possible using well-known asynchronous out-of-core techniques that permit I/O to and from multiple disk drives to be performed concurrently with the floating point operations.

6. FUTURE DEFENSE ELECTROMAGNETICS NEEDS

Goals for computational electromagnetics modeling capabilities in the defense area have been and remain driven by the design of low-observable aircraft and missiles. Some of these goals are now summarized.

6.1. *70 dB predictive dynamic range*

As noise-cancelling anechoic chambers become more sophisticated and attain effective quiet zones deeper than −70 dB, it is desired to extend numerical modeling capabilities to this dynamic range to balance theory and measurements. Clearly, larger predictive and measurement dynamic ranges permit structures of lower radar cross-section to be modeled and tested. Note that attainment of 70 dB predictive dynamic ranges is equivalent to the ability to suppress all sources of computational noise to amplitudes no larger than about 10^{-4} that of the incident wave. This will be a very difficult challenge for any computational electromagnetics model.

With respect to space-grid time-domain algorithms, a primary challenge will occur in the area of advanced radiation boundary conditions (RBCs). In comparison with today's codes, a 40-dB (100:1) improvement is needed here in reducing the effective reflection coefficient of the outer grid boundaries relative to outward propagating numerical modes. It is not clear that this will be possible without a fundamental advance in RBC theory or direct numerical emulation of the noise cancellation used in the 70-dB anechoic chambers.

6.2. *Modeling of complex and composite materials*

The usage of multilayer composites and cellular materials for structural and electromagnetic purposes in aerospace design has markedly increased. These materials can have inhomogeneities and anisotropies of their electric and magnetic properties at distance scales of a few microns, the thickness of one lamina in a composite sandwich. Further, the electric and magnetic properties can be functions of the frequency of radar illumination. Any conceivable electromagnetic analysis code will be very strongly challenged by the requirement to simultaneously model distance scales ranging over six orders of magnitude (from micrometers to meters) and frequencies ranging over three orders of magnitude (from megahertz to gigahertz).

In fact, it may be unfeasible in the time frame of the next decade to successfully attack the micrometers-to-meters distance-scale problem by direct modeling. Most likely, this problem will be approached by developing advanced electromagnetic field boundary conditions applied at the surface of complex composite media to nearly equivalence the field physics of the underlying media without having to refine the computational mesh beyond that used in the air region outside. If this is the case, the problem of modeling composite media in meshes is one of fundamental electromagnetic theory rather than numerical methods.

6.3. *Optimization of materials and shapes for RCS*

Analogous to CFD, the availability of increasingly sophisticated and accurate numerical analysis tools for RCS presents the possibility of optimizing target materials and shapes on the computer before any models are constructed. Space-grid time-domain models of scattering appear to be particularly useful for this purpose because of their potential for containing entire aircraft and their time-domain formulation. The latter permits modeling a very wideband [and even ultrawideband (UWB)] radar illumination in a single modeling run, as well as natural time-windowing of the scattering response to focus attention on the behavior of specific scattering centers.

For example, at least one published paper[48] reports an algorithm to automatically optimize the RCS of a structure using space-grid time-domain techniques. The algorithm of Ref. 48 optimizes broadband absorptive coatings for two-dimensional structures by embedding a FD-TD forward-scattering code in a numerical feedback loop with the Levenberg–Marquardt (LM) non-linear optimization routine. LM is used to adjust the many geometric and constitutive parameters that characterize the target, while FD-TD is used to obtain the broadband RCS response for each target adjustment. A recursive improvement process is established to minimize the broadband RCS response over a selected range of bistatic angles using the available engineering degrees of freedom. The solution is valid over the potentially broad bandwidth (frequency decade or more) of the illuminating pulse used in the FD-TD model.

This approach compactly treats the scatterer shape and coating specifications as a single point in an N-dimensional space (N-space) of geometrical and electrical parameters. By repeatedly recalculating the forward problem to obtain one or more figures of merit for the near or far-field response, this method implements a gradient-based search strategy in the N-space to obtain locally optimum monostatic or bistatic RCS reductions over the bandwidth of the illuminating plane wave pulse. More globally optimum searches can be conducted by seeding the algorithm with a variety of starting points in the N-space. The non-linear optimizer also permits adding constraints so that the search path in the N-space weights manufacturability and cost, and avoids possible forbidden zones.

Figure 2 illustrates the use of this method to synthesize an absorbing coating for a canonical two-dimensional structure, the infinite, perfectly conducting right-angle wedge subject to transverse magnetic (TM) illumination. As shown in Fig. 2a, the wedge coating is a single homogeneous 5 mm thick absorbing layer to the left and bottom of the wedge

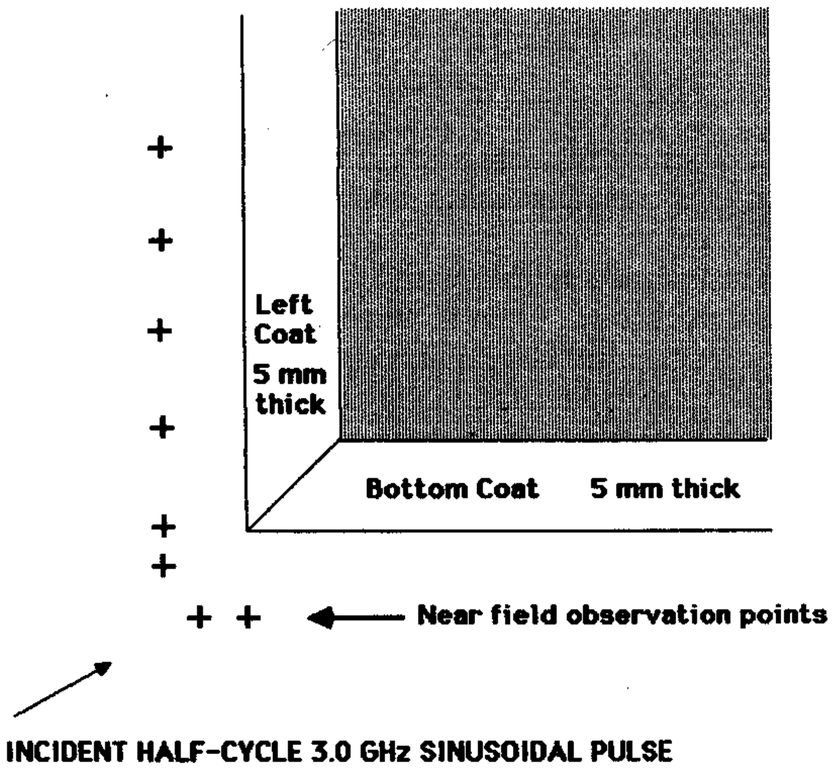

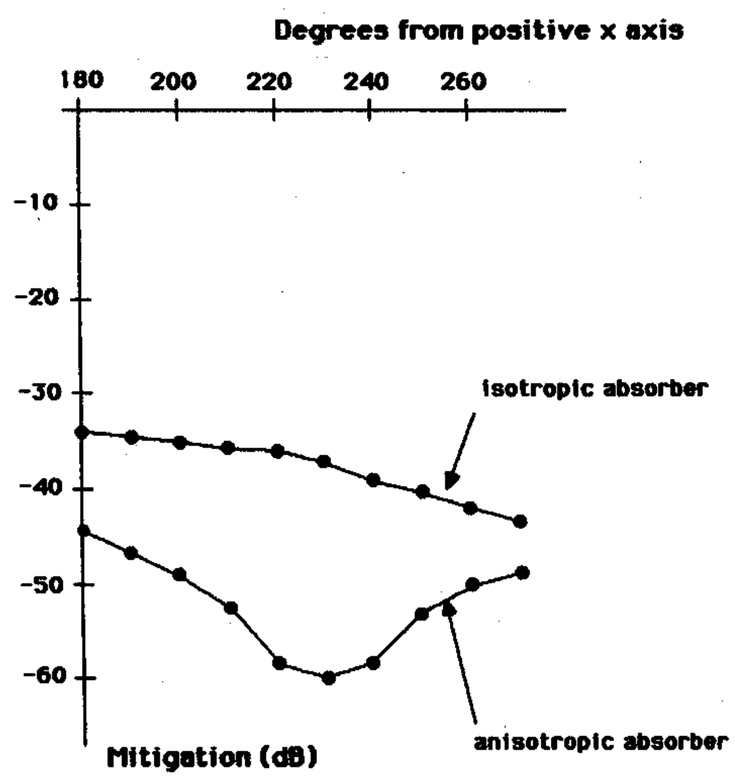

Fig. 2. FD-TD/LM synthesis of broadband absorbing coatings on an infinite conducting right-angle wedge, two-dimensional™ case: (a) wedge and coating geometry, showing the near-field observation points; (b) optimized mitigation of the broadband scattered pulse in the far field for bistatic angles bracketing the monostatic return, isotropic and anisotropic coating cases.

vertex, joined via a miter. In one case considered, the coating is assumed to be isotropic and independent of position, while in the other the coating is permitted to have an anisotropy of the magnetic loss that is dependent upon location (either in the left or bottom coat). The broadband illumination, a half-cycle 3.0 GHz sinusoidal pulse, is highly resolved everywhere by using a space discretization of $\lambda_0/200$. LM non-linear optimization is employed to minimize a weighted average of scattered near-field energy as observed at the eight near-field points indicated in Fig. 2a. From Fig. 2b, we see that the optimized broadband bistatic RCS mitigation in the far field (ratio of the peak scattered pulse power with coating to the peak scattered pulse power without coating) for bistatic angles bracketing the monostatic return is -34 to -42 dB for the isotropic coating and -44 to -60 dB for the anisotropic coating.

This case was purposefully selected to represent a coating N-space of low dimensionality, i.e. no coating layering was permitted. Given the simplicity of the coating examined here, it is likely that expanding the dimensionality of the automated search procedure would significantly increase the broadband RCS mitigation, increase the range of bistatic angles mitigated for RCS and decrease the sensitivity of the RCS mitigation to the illumination angle.

Methods such as the above appear to be ideal for implementation on massively parallel, multiple instruction multiple datastream (MIMD) computers. Here, systematic global searches of the N-space of interest could be implemented by assigning to each of the hundreds of processors (or groups of processors) a specific seed, or starting point, in the N-space. The searches could proceed independently of each other, culminating in an optimized engineering design for RCS.

6.4. *Integrated RCS and aerodynamics design and optimization*

In principle, the above ideas can be taken a large step further by performing simultaneous, linked modeling and optimization of RCS and aerodynamic performance, since these separate engineering goals can strongly mutually interact and even directly conflict. Needless to say, automated, integrated RCS/aero design is an ambitious goal—a true grand challenge—well worthy of the teraflop computers and 70 dB dynamic range electromagnetic modelers hopefully to come by the year 1997.

An interesting issue here is: "Should we use the same computational mesh for both the RCS model and the aero model?" At first glace this appears to be desirable, since target geometry and meshing could then be shared by both disciplines and the non-linear optimization software would deal with only a single geometry data base. However, it is less clear that the extraordinary 70 dB dynamic range needed by the electromagnetics model can be achieved by "shoehorning" Maxwell's equations into current CFD meshes. The physics involved in the two disciplines may be sufficiently different to mandate a Maxwell-specific mesh for the electromagnetics model. The computer storage and running time of the electromagnetics code and complexity of the umbrella non-linear optimization software may also factor into the choice of mesh for the electromagnetics model.

6.5. *Target identification*

An interesting observation is that the technique of embedding a space-grid time-domain Maxwell's solver within a non-linear optimization algorithm, considered above in the context of synthesizing scatterers having desired RCS properties, appears to be useful in reconstructing the shape (and even the composition) of a target from its broadband radar signature.[49]

Again, consider the FD-TD/LM non-linear optimization algorithm, but with the optimizer geared to replicate some finite measured impulsive scattering response rather than replicate a zero desired scattering response. Now, FD-TD generates a test pulse response for a parameterized trial target shape or composition, the test pulse is compared to the measured pulse, and an error signal is developed. Working on this error signal, the LM algorithm perturbs the original trial point in the N-space of parameters, effectively conducting a gradient search through this N-space. Upon repeated iterations, the trials ideally converge to the actual target geometry and composition. The advantage of working in the time domain is that causality can be exploited to permit progressive and cumulative target reconstruction as the incident pulse wavefront moves across the target. This reduces the complexity of reconstruction since only a portion of the target is being generated at each iteration.

Figure 3 provides examples of the ability of the FD-TD/LM non-linear optimization technique to exploit causality and reconstruct a dielectric J-shaped target from minimal two-dimensional TM near-field data contaminated by additive Gaussian noise.[49] Here, a single field observation point was assumed to be located approximately 10 target spans from the front vertex of the J-target, with the incident plane wave pulse having a spatial width comparable with the J-target span and headed toward the front vertex of the J. The principal *a priori* information provided to the optimizer here is the target composition: lossless dielectric ($\epsilon_r = 2.1$).

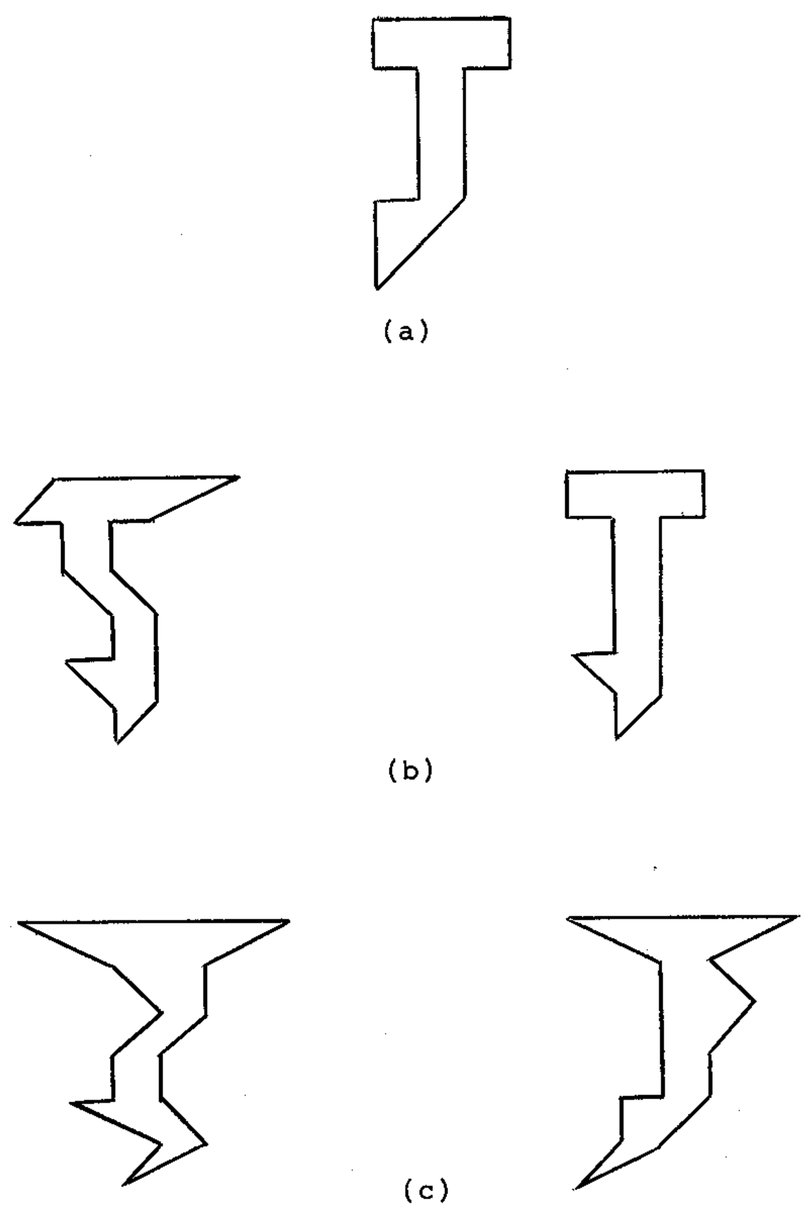

Fig. 3. Typical effects of Gaussian noise upon FD-TD/LM non-linear optimization inverse scattering reconstruction of a two-dimensional dielectric target having reentrant features: (a) $S/N = 40$ dB, exact reconstruction; (b) $S/N = 30$ dB, examples of imperfect reconstruction; (c) $S/N = 25$ dB, examples of imperfect reconstruction.

Figure 3 exemplifies hundreds of FD-TD/LM reconstruction attempts where varying samples of Gaussian noise (provided by a random number generator) are added to the simulated measured scattered waveform (a sequence of FD-TD-generated numbers). Using this technique, the probability of exact reconstruction of the J-shaped target has been estimated as a function of the signal-to-noise (S/N) power ratio. It has been found that the probability of exact reconstruction exceeds 0.9 when S/N ratios exceed 40 dB. For lower S/N ratios, the reconstruction process appears to degrade gracefully, as shown.

We see that space-grid time-domain Maxwell's solvers combined with non-linear optimizers that exploit causality hold promise for the classic inverse-scattering problem. Further progress awaits study of this problem by more groups in the Maxwell's equations gridding community. Perhaps this will occur in the next 5 years.

7. FUTURE DUAL-USE ELECTROMAGNETICS NEEDS

By the mid-1990s, we will be implementing space-grid time-domain Maxwell's solvers on the 0.1–1 Tflop supercomputers of the day to model the radar cross-section of entire low-observable fighter aircraft at frequencies up to at least 2 GHz through dynamic ranges up to 70 dB; but, perhaps of more importance to the interests of society, we will be using these same Maxwell's solvers implemented on the same supercomputers to model electromagnetic wave problems that arise in cutting-edge commercial applications.

This discussion will start with extensions of existing commercial applications of electromagnetic wave interactions and proceed to highly innovative applications that best represent the dual-use nature of modeling Maxwell's equations on large scales.

7.1. *Antenna design*

This area includes the design of UHF/microwave data links for worldwide personal wireless telephony, cellular communications, remote computing and advanced automotive electronics (particularly car location and navigation).

Here, we are seeing that space-grid time-domain Maxwell's solvers are permitting the modeling of complicated antennas, especially those having finite ground planes that cannot be analyzed using conventional frequency-domain analyses based upon the Green's function technique. Key recent examples include:

(1) Maloney *et al.*[34]—FD-TD models of body-of-revolution-type monopoles and conical monopoles over finite ground planes. Here, computed results

for the transient reflected waveforms in the feeding coaxial line and for the input impedances were found to agree with measurements to better than 1%.

(2) Katz *et al.*[36]—surface-conforming FD-TD models of two-dimensional waveguide-fed horn antennas and horn-excited parabolic reflectors. Here, the computed results for near-fields in the antenna apertures were found to agree with frequency-domain MoM numerical data to within 1% in magnitude and phase.

(3) Tirkas and Balanis[35]—surface-conforming FD-TD models of three-dimensional waveguide-fed horn antennas. Here, the computed results for far-field radiation patterns were found to agree very well with measurements over a 55-dB dynamic range.

(4) Thiele and Taflove[50]—in perhaps the most complex modeling so far, the authors are constructing three-dimensional FD-TD models of 6–18 GHz Vivaldi flares (tapered slot antennas) constructed from three-layer circuit board. Here, both single flares, double flares, quad elements comprised of perpendicular double-flares and arrays of up to eight quad elements are being modeled. The latter involve the solution of up to 60,000,000 vector field unknowns. Results are being obtained for radiation pattern and input impedance. The variation of the input impedance with phasing of the array of quad elements is also being studied.

As detailed FD-TD modeling proceeds in this area, it is possible that commercial application areas will include the design of mass-produced surface-conforming antennas for: homes (rooftop-mounted antennas for satellite reception); automobiles (rooftop-mounted antennas for two-way satellite communication, license-plate-mounted antennas for automated collision avoidance and programmed route-following); and laptop computers (computer-case-mounted antennas for two-way cellular and satellite communication).

7.2. *Microwave circuits*

Stripline microwave circuits, including filtering elements and couplers, are being studied for the first time by applying grid-based time-domain Maxwell's solvers. Key recent examples include:

(1) Sheen *et al.*[30]—FD-TD models of microstrip interconnects.

(2) Ko and Mittra[31]—three-dimensional FD-TD models yielding the broadband S-parameters of microstrip filters, couplers and hybrids.

This work is leading to the modeling of microwave and millimeter wave integrated circuits (MIMIC) in regimes of electrical size and complexity that cannot be handled by any existing finite-element or boundary integral method.

7.3. *Bioelectromagnetic systems*

Grid-based time-domain Maxwell's solvers are now being extensively applied in clinical settings for patient-specific electromagnetic hyperthermia. This technology uses electromagnetic absorption at RF, UHF, or microwave frequencies to heat cancerous tumors inside the human body, thereby rendering the tumors more vulnerable to ionizing radiation or chemotherapy. Recent examples of work include:

(1) Sullivan[19]—three-dimensional FD-TD models of RF hyperthermia for human patients.

(2) Piket-May *et al.*[20]—three-dimensional FD-TD models of UHF hyperthermia specifically tailored to patients by using computed tomography (CT) imaging to establish a three-dimensional dielectric medium data base unique to each patient's tissue structure.

This work is leading to the routine clinical usage of electromagnetic hyperthermia for cancer treatment. Time-domain solution of Maxwell's equations on grids is essential to this process because it permits an efficient, individual modeling of each patient to accommodate the electromagnetic field physics unique to his or her tissue geometry and selection of field applicators.

7.4. *Packaging and metallic interconnect design for digital circuits*

This area involves engineering problems in the propagation, crosstalk and radiation of electronic digital pulses, and has important implications in the design of the multi-layer circuit boards and multi-chip modules that are widely used in modern digital technology. Most existing computer-aided circuit design tools (primarily SPICE) are inadequate when digital clock speeds exceed about 250 MHz. These tools cannot deal with the physics of UHF/microwave electromagnetic wave energy transport (along metal surfaces like ground planes, or in the air away from metal paths) that predominate above 250 MHz. Effectively, electronic digital systems develop substantial analog wave effects when clock rates are high enough, and full-vector (full-wave) Maxwell's equations solvers become necessary for their understanding.

Key recent examples include:

(1) Liang *et al.*[28]—three-dimensional FD-TD modeling of picosecond pulse propagation along co-planar waveguides above gallium arsenide.

(2) Shibata and Sano[29]—three-dimensional FD-TD modeling of propagation along metal–insulator–semiconductor lines.

(3) Lam *et al.*[51]—three-dimensional FD-TD modeling of digital signal propagation and radiation for VLSI packaging.

(4) Maeda *et al.*[52]—three-dimensional FD-TD modeling of digital pulse propagation through vias in a three-layer circuit board.

(5) Piket-May *et al.*[53]—in perhaps the most complex modeling so far, the authors constructed three-dimensional FD-TD models of sub-nanosecond digital pulse propagation and crosstalk behavior in

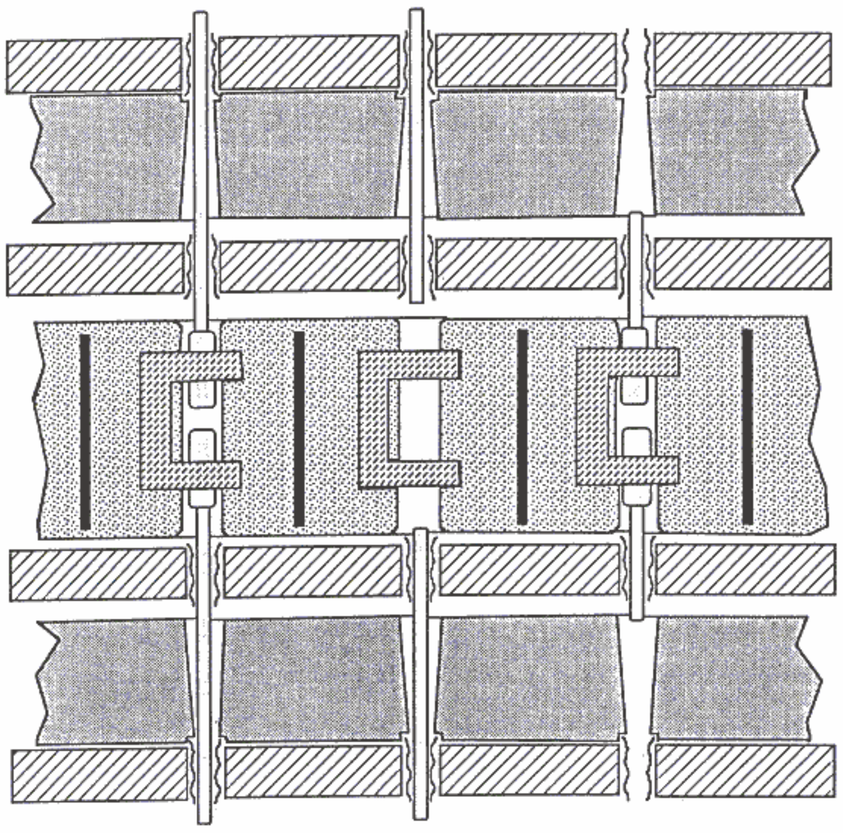

Fig. 4. Vertical cut through the four-circuit-board, three-connector geometry showing the via pins spaced 0.1 in apart.

modules consisting of four 22-layer circuit boards connected by three 100-pin connectors. The entire space was modeled with a uniform resolution of 0.004 in, permitting each layer, via and pin of the circuit boards and connectors to be modeled. A maximum of 60,000,000 vector field unknowns was solved per modeling run, a factor of perhaps 600 times larger than the capacity of the largest SPICE or finite-element CAD tool available. Color videos of digital signal propagation and crosstalk were constructed to vividly illustrate these phenomena.

Figure 4 depicts the geometry of the four-board, three-connector stack as seen in a vertical cut through the stack. Each 22-layer circuit board is shown as a cross-hatched horizontal slab, and each vertical via pin (spaced at a 0.1 in interval) is shown in proper relation to the surrounding boards and connectors. (Recall that each 0.004 in-thick metal–dielectric layer of each board is modeled.)

Figure 5 is a color plate showing the plan view of an outwardly propagating electromagnetic wave within a single 22-layer board generated by the passage of a sub-nanosecond pulse down one of the via pins. Although the relatively intense magnetic field adjacent to the excited via (shown by the yellow color) is quite localized, moderate-level magnetic fields (shown by light blue) emanate throughout the entire transverse cross-section of the board and link all of the adjacent via pins, shown as dark dots in a diamond pattern. The complete color video of this phenomenon shows repeated bursts of outward propagating waves linking all points within transverse cross-sections of the board as the digital pulse passes vertically through the 22 metal–dielectric–metal layers of the board.

Figure 6 is a color plate showing the magnitude and direction of currents instantaneously flowing along the vertical cross-section of Fig. 4 for a sub-nanosecond digital pulse assumed to excite a single vertical via pin in the upper 22-layer board. The currents were calculated in a post-processing step by numerically evaluating the curl of the magnetic field obtained from the three-dimensional FD-TD model. The color red was selected to denote downward-directed current, while the color green was selected to denote upward-directed current. At the time of this visualization, current had proceeded down the excited via through all four boards and all three connectors; but upward-directed (green) current is seen to flow on the adjacent vias. This represents undesired ground-loop coupling to the digital circuits using these vias. Ironically, the far-left-hand and far-right-hand vias showing downward-directed (red) currents were designated by the designers of this structure to be the ground return pins and should have been the only pins carrying upward-directed (green) current. In other words, this interconnection module wound up working nearly in an opposite manner relative to what its designers had intended.

This work is leading to the direct time-domain Maxwell's equations modeling of the metallic interconnects and packaging of general-purpose digital circuits operating at clock speeds about 250 MHz. From the example shown, it is clear that the analog coupling effects for such devices can be so complex that there may be no way to design them—no way to make them work in a timely and reliable manner—without such modeling.

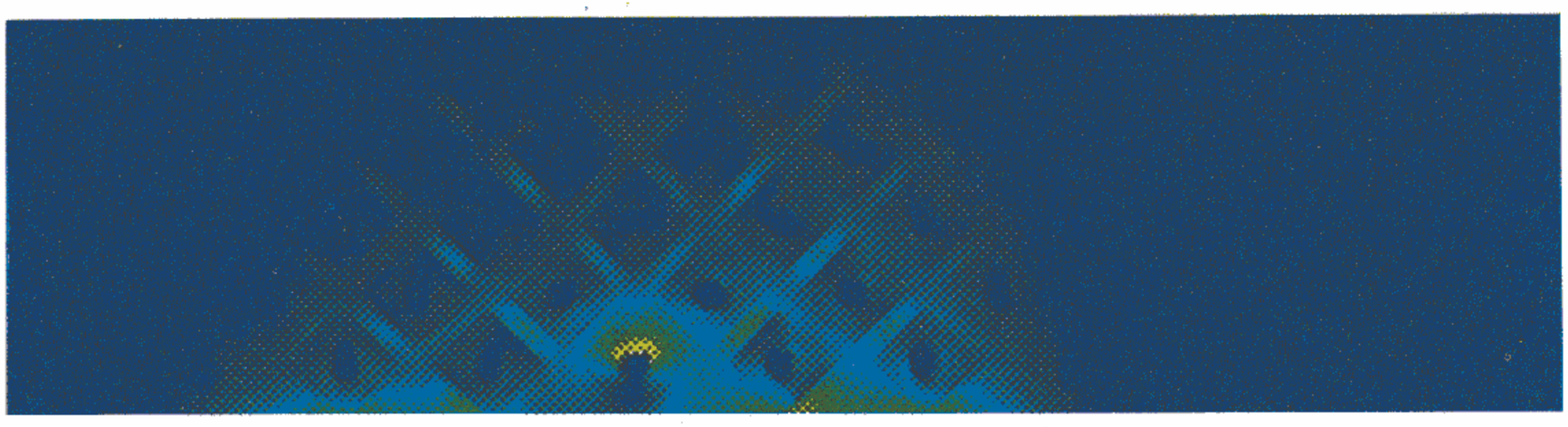

Fig. 5. Color plate showing the plan view of an outwardly propagating electromagnetic wave within a single circuit board of Fig. 4 generated by the passage of a sub-nanosecond pulse down one of the via pins. Color scale: yellow = maximum; green = moderate; dark blue = negligible.

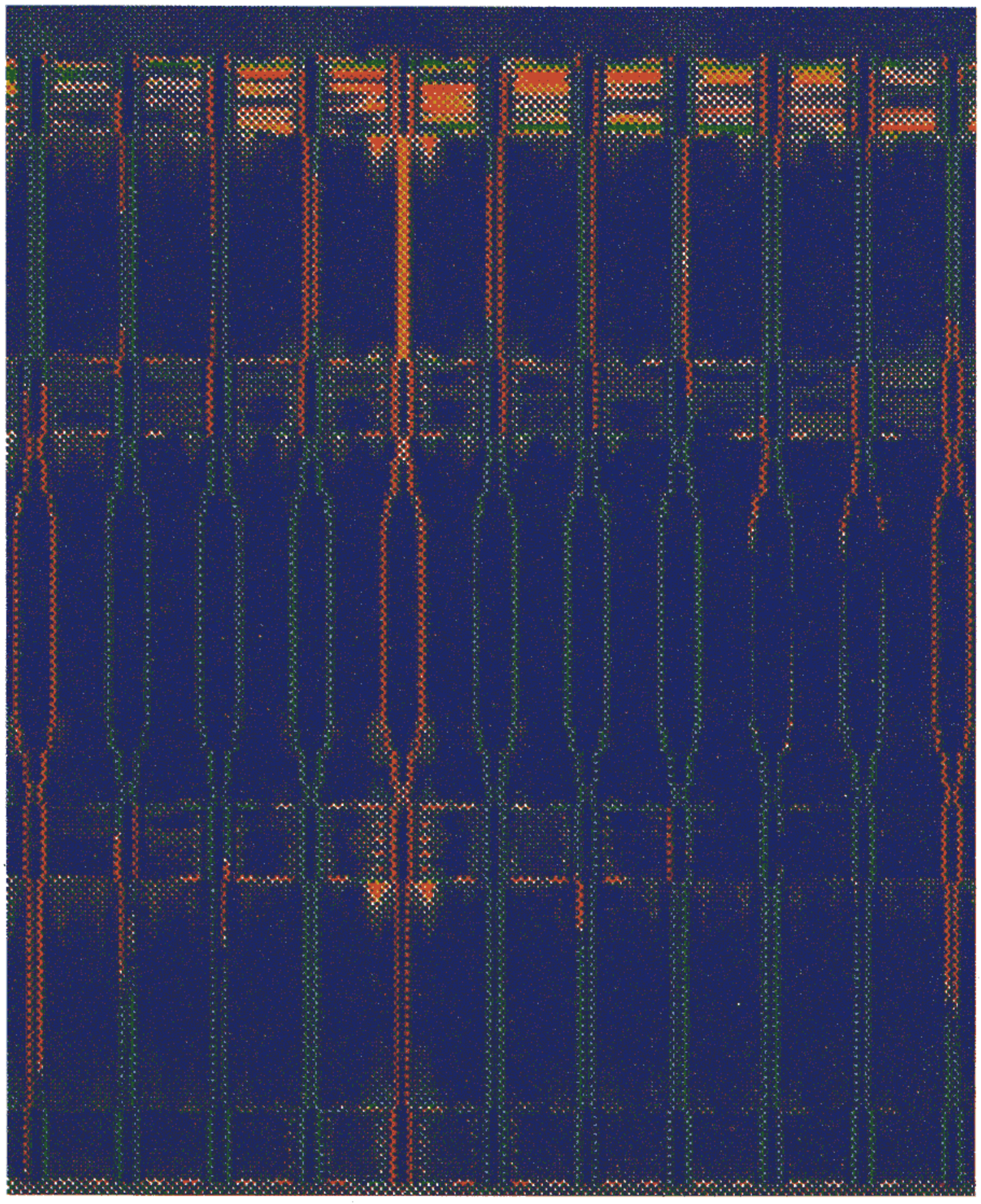

Fig. 6. Color plate showing the magnitude and direction of currents instantaneously flowing along the vertical cross-section of Fig. 4 for a sub-nanosecond digital pulse assumed to excite a single vertical via pin in the upper 22-layer board. Color scale: red = net downward-directed current; green = net upward-directed current; dark blue = negligible.

7.5. *Incorporation of models of active devices*

It is a short distance from modeling device packaging and interconnects, as discussed above, to including the active devices themselves. Work has begun in this area. The best examples are:

(1) Sano and Shibata[37]—incorporation of a self-consistent drift-diffusion charge-transport model of gallium arsenide in the three-dimensional FD-TD solver. This work modeled picosecond-regime pulse generation for an optically excited gallium arsenide device.

(2) El Ghazaly *et al.*[38]—incorporation of a self-consistent Monte Carlo charge-transport model of gallium arsenide in the three-dimensional FD-TD solver. This work also modeled picosecond-regime pulse generation for an optically excited gallium arsenide device.

(3) Sui *et al.*[41]—two-dimensional FD-TD modeling of lumped-circuit elements (resistors, inductors, capacitors, diodes and transistors).

By 1995, this work will probably lead to the incorporation of SPICE models of arbitrary linear and non-linear circuit elements into three-dimensional space-grid time-domain Maxwell's solvers. This will expand full-vector electromagnetic modeling of digital interconnects to include the voltage–current characteristics of the connected logic devices. It should result in a virtual replacement of SPICE for most problems involved in digital interconnect design above 250 MHz.

A recently initiated 3-year cooperative program between Cray Research and Los Alamos National Laboratory recognizes the possibility that the design of the digital microchips themselves will mandate

full-vector EM modeling, especially when clock speeds exceed 3 GHz. In this regime, wave propagation and coupling effects within the chips may render their operation just as problematic as that of today's circuit board modules operating at 300 MHz.

Subsequently, the Cray/Los Alamos program seeks to explore Maxwell's equations modeling of digital chips having clock speeds well above 10 GHz. The reasoning here is that when the logic pulse rise time becomes comparable with the charge transport time, existing approaches for modeling semiconductors which assume a quasi-static formulation for Maxwell's equations (the Poisson equation) will no longer have validity. In this regime, the simple circuit concept of a digital signal toggling a transistor may have to be considered at the most elemental level. Namely, the digital signal and transistor actually comprise a three-dimensional electromagnetic pulse scattering geometry: the digital signal is really a three-dimensional propagating field distribution having a specific temporal response and the transistor is really a three-dimensional charge density distribution that reacts non-linearly to the impinging electromagnetic pulse. Self-consistent Maxwell's equations field transport and semiconductor charge transport modeling are required to properly understand this non-linear scattering situation.

7.6. *Application to all-optical devices*

Work has begun to appear on first-principles modeling of the propagation and switching of femtosecond optical pulses in non-linear dispersive media. Again, time-domain grid-based Maxwell's solvers are being used:

(1) Joseph *et al.*[33]—demonstrated and rigorously validated an efficient one-dimensional FD-TD analysis of femtosecond pulse propagation and reflection effects for a linear Lorentz (resonant dispersive) medium. This work pioneered direct Maxwell's equations modeling of second-order dispersion, providing extremely accurate physics over instantaneous bandwidths of literally d.c. to light for reflection coefficients and Sommerfeld and Brillouin impulsive precursors.

(2) Goorjian and Taflove[39]—demonstrated an efficient one-dimensional FD-TD analysis of femtosecond optical soliton propagation and collision in a second-order non-linear dispersive medium. This work obtained for the first time optical solitons from Maxwell's equations, with quantum physics such as the Kerr and Raman interactions incorporated into the Maxwell's equations at distance scales larger than about 10 nm.

(3) Ziolkowski and Judkins[40]—two-dimensional FD-TD analysis of femtosecond optical pulse propagation and self-focusing in a first-order non-linear dispersive medium.

Consider qualitatively the key results of Ref. 39. Fig. 7a depicts the FD-TD computed propagation of a 50 fs duration infrared optical pulse observed at

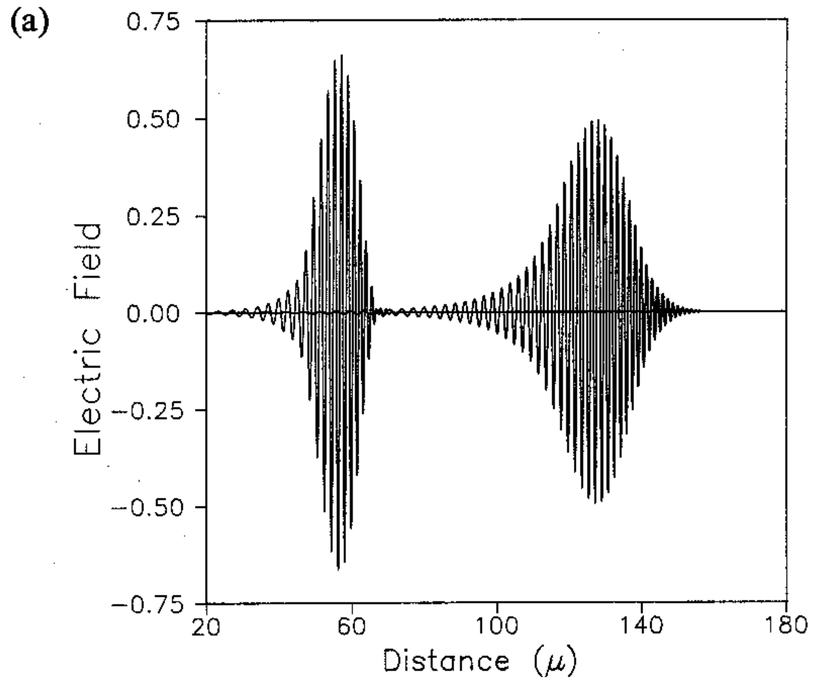

Fig. 7. FD-TD computed propagation of a 50 fs duration infrared optical pulse observed at propagation distances of 55 and 126 μm from the source in a medium having anomalous dispersion due to a single Lorentzian relaxation: (a) linear case, showing pulse attenuation, broadening, and frequency modulation; (b) dispersive non-linear case, showing the formation of a soliton pulse and precursor.

propagation distances of 55 and 126 μm from the source in a linear medium having anomalous dispersion. Note pulse broadening, diminishing amplitude and carrier frequency modulation ($>f_c$ on the leading side, $<f_c$ on the trailing side) which causes an asymmetrical shifting of the envelope, a higher-order dispersive effect. In Fig. 7b, sufficient non-linearity is introduced to yield a soliton that retains its amplitude and width when observed at the same propagation distances as Fig. 7a. However, a low-amplitude precursor is seen to move out ahead of the soliton. The carrier frequency of this precursor is upshifted to approximately 3.6 times that of the main pulse.

Figure 8 depicts the Fourier spectrum of the solitons shown in Fig. 7b. The figure shows a red shift and sharpening of the spectrum as the pulse propagates. This red shift is predicted due to the Raman effect occurring as a higher-order dispersive non-linearity modeled by the non-linear Maxwell's equations solver.

Finally, Ref. 39 considers the collision of two counter-propagating solitons. Each is identical and

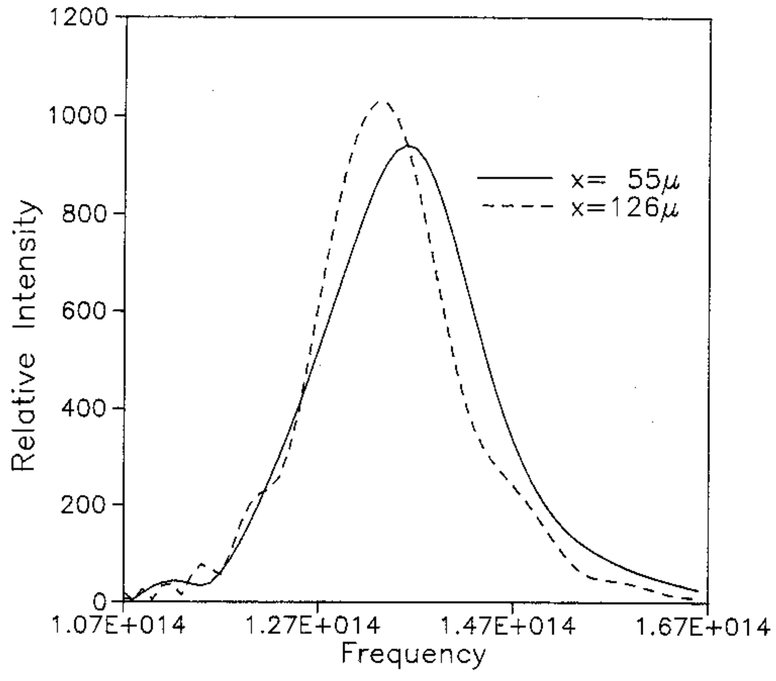

Fig. 8. Red shift of the Fourier spectrum of the propagating soliton of Fig. 7b.

has all of the parameters of the previous case. As is characteristic of colliding solitons, after the collisions the pulses separate without changing their general appearance. However, there are lagging phase shifts due to the collision, up to 31° for the carrier in the precursor. To illustrate this, Fig. 9 plots the space dependence of the central part of the precursor for the uncollided case and the collided case. Such phase shifts, not easily detected by previous theory, may be a basis for optical switching devices.

Unlike all previous soliton theory based upon the pulse-envelope approach, the direct Maxwell's equations model of Ref. 39 assumes nothing about the homogeneity or isotropy of the optical medium, the magnitude of its non-linearity, the nature of its ω–β variation, or the shape or duration of the optical pulse. By retaining the optical carrier, the new Maxwell's equations method solves for fundamental quantities—the optical electric and magnetic fields in space and time—rather than a non-physical envelope function. Thus, it is extendible to full-vector optical fields in two and three dimensions to permit rigorous boundary value problem studies of non-linear vector-wave polarization, diffraction, scattering and interference effects. This is being actively pursued.

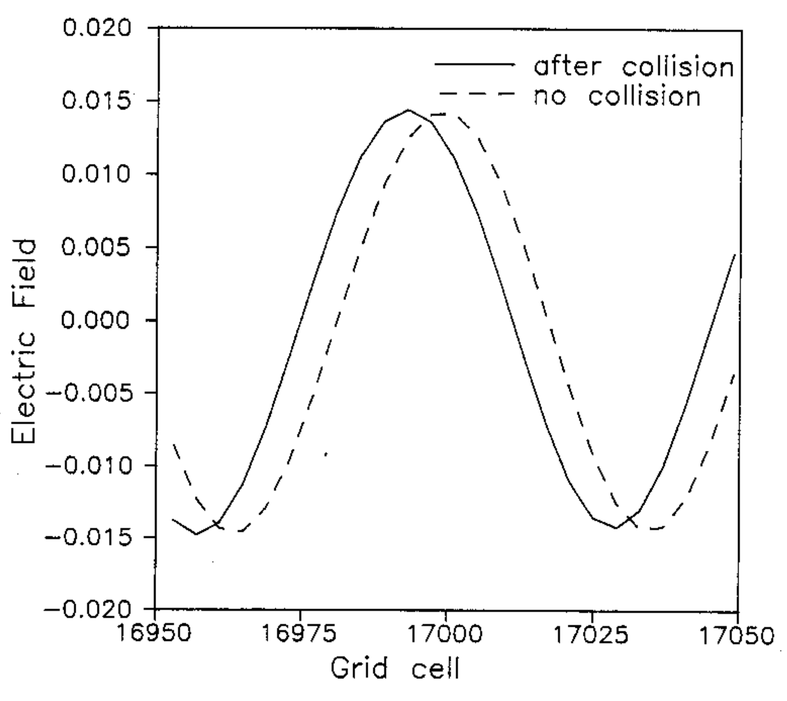

Fig. 9. Phase lag of the precursor pulse as a result of counterpropagating soliton–soliton collision.

This work may lead to the modeling of all-optical digital logic devices switching potentially in 10–50 fs at room temperature. This is about 1000 times faster than the best transistor today and 100 times faster than a Josephson junction operating under liquid helium. The implications may be profound for the realization of "optonics", a proposed successor technology to electronics in the 21st century that would integrate optical fiber interconnects and all-optical processors into systems of unimaginable information processing capability.

8. CONCLUSIONS

Supercomputers of the mid-1990s, which promise to achieve rates from 0.1 to 1 Tflop, will permit us to attack some "grand challenges" in electromagnetics. One such "challenge" remains from the RCS technology side—the airplane-in-the-grid. In fact, using the new class of machines and the new class of space-grid time-domain Maxwell's solvers, it will certainly be possible to obtain whole low-observable fighter-airplane models in the 1–3 GHz range and jet-engine-inlet models up to perhaps 5–10 GHz, with predictive dynamic ranges up to 70 dB. In addition, time-domain non-linear optimization algorithms will probably be used to achieve engineering goals with respect to observability and aerodynamics. But, of arguably more importance to society, the same algorithms implemented on the same computers could attack other "grand challenges" in electromagnetics:

- the satellite-antenna-in-the-grid;
- the cancer-patient-in-the-grid;
- the digital-microchip-module-in-the-grid;
- the microwave/millimeter wave integrated circuit-in-the-grid;
- the array-of-picosecond-transistors-in-the-grid;
- the femtosecond-all-optical-switch-in-the-grid, etc.

I assert that ultra-large-scale solution of Maxwell's equations using time-domain grid-based approaches may be fundamental to the advancement of our technology as we continue to push the envelope of the ultra-complex and the ultra-fast. Simply speaking, Maxwell's equations provide the physics of electromagnetic phenomena from d.c. to light and their accurate modeling is essential to understand high-speed signal effects having wave transport behavior. Let us aim for the computational unification of:

- full-vector electromagnetic waves in three dimensions;
- charge transport in transistors, Josephson junctions and electro-optic devices;
- surface and volumetric wave dispersions, including those of superconductors; and
- non-linearities due to quantum effects.

Then, we can attack some computational "grand challenges" to directly benefit our society.

Acknowledgements—The author acknowledges the invaluable assistance of his collaborators, Professor Korada Umashankar of the University of Illinois at Chicago, Dr Peter Goorjan of NASA Ames and Dr Evans Harrigan of Cray Research. He also acknowledges the assistance of his graduate students, Rose Joseph, Dan Katz, Melinda Piket-May, Chris Reuter and Eric Thiele, as well as his undergraduate research students Peter Anvin, Susan Hagness and Ann Komaromi. The author was supported in part by NASA Ames University Consortium Joint Research Interchange Grants NCA2 561 and 562, Office of Naval Research Contract N00014-88-K-0475, and Cray Research, Inc.

REFERENCES

1. R. F. Harrington, *Field Computation by Moment Methods*, Macmillan, New York, 1968.
2. K. R. Umashankar, "Numerical analysis of electromagnetic wave scattering and interaction based on frequency-domain integral equation and method of moments techniques," *Wave Motion* **10,** 493 (1988).
3. J. B. Keller, "Geometrical theory of diffraction," *Journal of the Optical Society America* **52,** 116 (1962).
4. R. G. Kouyoumjian and P. H. Pathak, "A uniform geometrical theory of diffraction for an edge in a perfectly conducting surface," *Proceedings of the IEEE* **62,** 1448 (1974).
5. J. P. Brooks, K. K. Ghosh, E. Harrigan, D. S. Katz and A. Taflove, "Progress in Cray-based algorithms for computational electromagnetics," in *Progress in Electromagnetics Research* (*PIER*) edited by T. Cwik, Vol. 7, Elsevier, New York, 1992.
6. K. S. Yee, "Numerical solution of initial boundary value problems involving Maxwell's equations in isotropic media," *IEEE Transactions Antennas and Propagation* **14,** 302 (1966).
7. A. Taflove and M. E. Brodwin, "Numerical solution of steady-state electromagnetic scattering problems using the time-dependent Maxwell's equations," *IEEE Transactions Microwave Theory Tech.* **23,** 623 (1975).
8. A. Taflove and M. E. Brodwin, "Computation of the electromagnetic fields and induced temperatures within a model of the microwave-irradiated human eye," *IEEE Transactions Microwave Theory Tech.* **23,** 888 (1975).
9. R. Holland, "Threde: a free-field EMP coupling and scattering code," *IEEE Transactions Nuclear Science* **24,** 2416 (1977).
10. K. S. Kunz and K. M. Lee, "A three-dimensional finite-difference solution of the external response of an aircraft to a complex transient EM environment I: the method and its implementation," *IEEE Transactions Electromagnetic Compat.* **20,** 328 (1978).
11. A. Taflove, "Application of the finite-difference time-domain method to sinusoidal steady-state electromagnetic penetration problems," *IEEE Transactions Electromagnetic Compat.* **22,** 191 (1980).
12. G. Mur, "Absorbing boundary conditions for the finite-difference approximation of the time-domain electromagnetic field equations," *IEEE Transactions Electromagnetic Compat.* **23,** 377 (1981).
13. K. R. Umashankar and A. Taflove, "A novel method to analyze electromagnetic scattering of complex objects," *IEEE Transactions Electromagnetic Compat.* **24,** 397 (1982).
14. A Taflove and K. R. Umashankar, "Radar cross section of general three-dimensional scatterers," *IEEE Transactions Electromagnetic Compat.* **25,** 433 (1983).
15. G. A. Kriegsmann, A. Taflove and K. R. Umashankar, "A new formulation of electromagnetic wave scattering using an on-surface radiation boundary condition approach," *IEEE Tranactions Antennas and Propagation* **35,** 153 (1987).
16. T. G. Moore, J. G. Blaschak, A. Taflove and G. A. Kriegsmann, "Theory and application of radiation boundary operators," *IEEE Transactions Antennas and Propagation* **36,** 1797 (1988).
17. D. T. Borup, D. M. Sullivan and O. P. Gandhi, "Comparison of the FFT conjugate gradient method and the finite-difference time-domain method for the 2-D absorption problem," *IEEE Tranactions Microwave Theory Tech.* **35,** 383 (1987).
18. D. M. Sullivan, O. P. Gandhi and A. Taflove, "Use of the finite-difference time-domain method in calculating EM absorption in man models," *IEEE Transactions Biomedical Engineering* **35,** 179 (1988).
19. D. M. Sullivan, "Three-dimensional computer simulation in deep regional hyperthermia using the finite-difference time-domain method," *IEEE Transactions Microwave Theory Tech.* **38,** 204 (1990).
20. M. J. Piket-May, A Taflove, W.-C. Lin, D. S. Katz, V. Sathiaseelan and B. Mittal, "Initial results for automated computational modeling of patient-specific electromagnetic hyperthermia," *IEEE Transactions Biomedical Engineering* **39,** 226 (1992).
21. K. R. Umashankar, A. Taflove and B. Beker, "Calculation and experimental validation of induced currents on coupled wires in an arbitrary shaped cavity," *IEEE Transactions Antennas and Propagation* **35,** 1248 (1987).
22. A. Taflove, K. R. Umashankar, B. Beker, F. Harfoush and K. S. Yee, "Detailed FD-TD analysis of electromagnetic fields penetrating narrow slots and lapped joints in thick conducting screens," *IEEE Transactions Antennas and Propagation* **36,** 247 (1988).
23. T. G. Jurgens, A. Taflove, K. R. Umashankar and T. G. Moore, "Finite-difference time-domain modeling of curved surfaces," *IEEE Tranactions Antennas and Propagation* **40,** 357 (1992).
24. A. C. Cangellaris, C. C. Lin and K. K. Mei, "Point-matched time-domain finite element methods for electromagnetic radiation and scattering," *IEEE Transactions Antennas and Propagation* **35,** 1160 (1987).
25. V. Shankar, A. H. Mohammadian and W. F. Hall, "A time-domain finite-volume treatment for the Maxwell's equations," *Electromagnetics* **10,** 127 (1990).
26. B. J. McCartin, L. J. Bahrmasal and G. Meltz, "Application of the control region approximation to two-dimensional electromagnetic scattering," in *Progress in Electromagnetics Research* (edited by M. A. Morgan), Vol. 2, Ch. 5, Elsevier, New York, 1990.
27. N. K. Madsen and R. W. Ziolkowski,"A three-dimensional modified finite volume technique for Maxwell's equations," *Electromagnetics* **10,** 147 (1990).
28. G.-C. Liang, Y.-W. Liu and K. K. Mei, "Full-wave analysis of coplanar waveguide and slotline using the time-domain finite-difference method," *IEEE Transactions Microwave Theory Tech.* **37,** 1949 (1989).
29. T. Shibata and E. Sano, "Characterization of MIS structure coplanar transmission lines for invesigation of signal propagation in integrated circuits," *IEEE Transactions Microwave Theory Tech.* **38,** 881 (1990).
30. D. M. Sheen, S. M. Ali, M. D. Abouzahra and J. A. Kong, "Application of the three-dimensional finite-difference time-domain method to the analysis of planar microstrip circuits," *IEEE Transactions Microwave Theory Tech.* **38,** 849 (1990).
31. W. L. Ko and R. Mittra, "A combination of FD-TD and Prony's methods for analyzing microwave integrated circuits," *IEEE Transactions Microwave Theory Tech.* **39,** 2176 (1991).
32. R. Luebbers, F. P. Hunsberger, K. S. Kunz, R. B. Standler and M. Schneider, "A frequency-dependent finite-difference time-domain formulation for dispersive materials," *IEEE Transactions Electromagnetic Compat.* **32,** 222 (1990).

33. R. M. Joseph, S. C. Hagness and A. Taflove, "Direct time integration of Maxwell's equations in linear dispersive media with absorption for scattering and propagation of femtosecond electromagnetic pulses," *Optics Letters* **16,** 1412 (1991).
34. J. G. Maloney, G. S. Smith and W. R. Scott, Jr, "Accurate computation of the radiation from simple antennas using the finite-difference time-domain method," *IEEE Transactions Antennas and Propagation* **38,** 1059 (1990).
35. P. A. Tirkas and C. A. Balanis, "Finite-difference time-domain technique for radiation by horn antennas," 1991 *IEEE Antennas and Propagation Society International Symposium Digest*, Vol. 3, pp. 1750–1753, London, Ontario, Canada, 1991.
36. D. S. Katz, M. J. Piket-May, A. Taflove and K. R. Umashankar, "FD-TD analysis of electromagnetic wave radiation from systems containing horn antennas," *IEEE Transactions Antennas and Propagation* **39,** 1203 (1991).
37. E. Sano and T. Shibata, "Fullwave analysis of picosecond photoconductive switches," *IEEE Journal Quantum Electronics* **26,** 372 (1990).
38. S. M. El-Ghazaly, R. P. Joshi and R. O. Grondin, "Electromagnetic and transport considerations in subpicosecond photoconductive switch modeling," *IEEE Transactions Microwave Theory Tech.* **38,** 629 (1990).
39. P. M. Goorjian and A. Taflove, "Direct time integration of Maxwell's equations in nonlinear dispersive media for propagation and scattering of femtosecond electromagnetic solitons," *Optics Letters* **17,** 180 (1992).
40. R. W. Ziolkowski and J. B. Judkins, "Full-wave vector Maxwell equation modeling of the self-focusing of ultrashort optical pulses in a nonlinear Kerr medium exhibiting a finite response time," *Journal Optical Society of America B*, submitted.
41. W. Sui, D. A. Christensen and C. H. Durney, "Extending the two-dimensional FD-TD method to hybrid electromagnetic systems with active and passive lumped elements,"*IEEE Transactions Microwave Theory Tech.* **40,** 724 (1992).
42. A. C. Ludwig, General Research Corporation, private communication.
43. S. W. Lee (ed.), *High Frequency Scattering Data Book*, Electromagnetic Laboratory, University of Illinois at Urbana-Champaign, 1989.
44. K. R. Umashankar, S. Nimmagadda and A. Taflove, "Numerical analysis of electromagnetic scattering by electrically large objects using spatial decomposition technique," *IEEE Transactions Antennas and Propagation*, in press.
45. A. T. Perlik, T. Opsahl and A. Taflove, "Predicting scattering of electromagnetic fields using FD-TD on a Connection Machine," *IEEE Transactions Magnetics* **25,** 2910 (1989).
46. J. E. Patterson, T. Cwik, R. D. Ferraro, N. Jacobi, P. C. Liewer, T. G. Lockhart, G. A. Lyzenga, J. W. Parker and D. A. Simoni, "Parallel computation applied to electromagnetic scattering and radiation analysis," *Electromagnetics* **10,** 21 (1990).
47. D. S. Katz, A. Taflove, J. P. Brooks and E. Harrigan, "Large-scale methods in computational electromagnetics," in *Cray Channels*, Cray Research, 1991.
48. M. A. Strickel and A. Taflove, "Time-domain synthesis of broadband absorptive coatings for two-dimensional conducting targets," *IEEE Transactions Antennas and Propagation* **38,** 1084 (1990).
49. M. A. Strickel, A. Taflove and K. R. Umashankar, "Finite-difference time-domain formulation of an inverse scattering scheme for remote sensing. Part II—Two-dimensional case: conducting and dielectric targets," *Journal of Electromagnetic Waves and Applications*, in press.
50. E. Thiele and A. Taflove, "FD-TD analysis of Vivaldi tapered slot antennas," in preparation.
51. C. W. Lam, S. M. Ali, R. T. Shin and J. A. Kong, "Radiation from discontinuities in VLSI packaging structures," *Proceedings of the Progress in Electromagnetics Research Symposium*, Boston, Massachusetts, p. 567, July 1991.
52. S. Maeda, T. Kashiwa and I. Fukai, "Full wave analysis of propagation characteristics of a through hole using the finite-difference time-domain method," *IEEE Transactions Microwave Theory Tech.* **39,** 2154 (1991).
53. M. Piket-May and A. Taflove, "First-principles supercomputing simulation of crosstalk in high-speed digital interconnects," 1992 Joint Symposia, URSI Radio Science Meeting Digest, p. 451, Chicago, IL, 1992.